Contents lists available at UGC-CARE

International Journal of Pharmaceutical Sciences and Drug Research

[ISSN: 0975-248X; CODEN (USA): IJPSPP]

journal home page : http://ijpsdr.com/index.php/ijpsdr

Research Article

Development and Characterization of Ultrasound-assisted PLGA Nanobubbles for the Triggered Delivery of Pemigatinib by Design of Experiments

P Nandini[1], DVRN Bhikshapathi[1*], M Viswaja[2], P Mamatha[2]

[1]*BirTikandrajit University, Canchipur, Imphal West, Manipur, India.*
[2]*TRR College of Pharmacy, Meerpet, Hyderabad, Telangana, India.*

ARTICLE INFO

Article history:
Received: 21 March, 2024
Revised: 24 April, 2024
Accepted: 11 May, 2024
Published: 30 May, 2024

Keywords:
Pemigatinib, Metastatic cholangiocarcinoma, Nanobubbles, Sonication distance, Droplet size, Polydispersity index, Central composite design.

DOI:
10.25004/IJPSDR.2024.160312

ABSTRACT

This study used a central composite design (CCD) to evaluate how the independent attributes—sonication distance (X_1), amplitude (X_2), time (X_3), and power (X_4)—impacted two outcomes—droplet size (Y1) and polydispersity index (PDI) (Y2). The time-consuming and inefficient "changing one factor at a time" approach would have been an option for this multifactor optimization, but we opted against it since we wanted to be sure we had the best possible values. Here, a mathematical model of the combined influence of the processing elements led to the selection of a CCD, which is known to be significantly more dependable. Using a double emulsion technique, we created and fine-tuned a drug delivery system consisting of nanobubbles loaded with pemigatinib. Pemigatinib nanobubbles were studied for their shape, surface charge, and particle size to determine their physicochemical characteristics and found that they were spherical with the zeta potential (ZP) and particle size of -25.3 ± 2.98 and 38.53 ± 2.14, respectively. Pemigatinib-loaded nanobubbles were also tested for their release behaviors and drug encapsulation effectiveness. Finally, we tried to study the anti-tumor activity and cellular absorption of poly (lactic-co-glycolic acid) nanobubbles-pemigatinib *in-vitro*.

INTRODUCTION

A rare and aggressive bile duct cancer called cholangiocarcinoma is treated with pemigatinib when it spreads locally or metastatically. It inhibits fibroblast growth factor receptors (FGFR) with high specificity. Cholangiocarcinoma and other cancers modify or overexpress these receptors.[1] Pemigatinib stops downstream signaling pathways that support cell growth and survival by binding to the FGFR's adenosine triphosphate (ATP)-binding site. This reduces tumor cell proliferation and promotes tumor cell demise. Pemigatinib might be an activeaction for cholangiocarcinoma subjects with FGFR mutations or overexpression due to its specific targeting of FGFRs. As with targeted medicines, Pemigatinib resistance is a key issue. Strategies to avoid this difficulty are being researched.[2,3] After a clinical trial showed that pemigatinib enhanced progression-free survival related to normal chemotherapy in formerly cured advanced cholangiocarcinoma subjects, the Food and Drug Administration (FDA) accepted it in April 2020. Pemigatinib causes high phosphate levels, hair loss, weariness, nausea, and diarrhea. Once a day, a tablet should be taken at blank stomach an hour previously or 2 hours after a meal. Following a doctor's dosing instructions and reporting adverse effects is critical.[4] Pemigatinib has limited water solubility, 0.0015 mg/mL at 25°C. Designing

***Corresponding Author:** Dr. DVRN Bhikshapathi

Address: BirTikandrajit University, Canchipur, Imphal West, Manipur, India.

Email ✉**:** dbpathi71@gmail.com

Tel.: +91-9848514228

Relevant conflicts of interest/financial disclosures: The authors declare that the research was conducted in the absence of any commercial or financial relationships that could be construed as a potential conflict of interest.

oral formulations is difficult due to its weak solubility, restricted permeability, and chemical characteristics.[5] Pemigatinib bioavailability (BA) depends on the patient's age, sex, weight, health, and drug formulation and dosage.[6] The compound's high aqueous insolubility reduces gastrointestinal absorption and BA. Due to these formulation issues, pemigatinib tablets contain excipients that improve solubility and BA. Note that hydroxypropyl-beta-cyclodextrin (HPβCD), a water-soluble cyclic sugar, forms inclusion complexes with pemigatinib, improving its solubility and dissolution rates. Croscarmellose sodium, a superdisintegrant, speeds tablet breakdown and medication release in the gastrointestinal system.[7] Despite these efforts to improve solubility andBA, some patients may have formulation-related adverse effects such as nausea and vomiting. Patient-specific factors like health state, concurrent medications, and nutrition can also affect pemigatinib absorption and efficacy.[8]

Nano formulations,[9] cyclodextrin complexation,[10] salt formation,[11] prodrug approach,[12] co-solvent systems,[13] and others could improve pemigatinib's solubility, stability, and BA. These different formulations may improve pemigatinib's pharmacokinetic (PK) and pharmacodynamic (PD) qualities, making it a better treatment for FGFR-altered cancer patients. Each method has its drawbacks; thus more research is needed to assess their efficacy for pemigatinib. Studies reveal that nanotechnology-based drug delivery methods may improve pemigatinib's PK and PD. Further study is needed to discover the best pemigatinib formulation and delivery technique and to measure the safety and efficacy of nanotechnology-oriented drug delivery methods in preclinical and clinical investigations. As per the up-to-date studies, we can find that, pemigatinib nanoparticle creation and utilization are poorly documented. While pemigatinib nanoparticle development is still early, in this study we investigated pemigatinib nanoparticle-based drug delivery systems to improve its solubility, BA, and cancer treatment efficacy.[14,15]

Nanobubble technology has various advantages over other nano-delivery systems, including versatile drug administration, controlled release, non-toxicity and biocompatibility, improved biological barrier penetration, and improved imaging. Overall, nanobubble technology seems promising for drug delivery and imaging. Its unique features make it a versatile and effective drug delivery platform. Nanobubbles have a gas core and a lipid or polymer shell that can carry medications and target tissues or cells. When stimulated by ultrasound, nanobubbles release the therapeutic payload.[16,17] The capacity of nanobubbles to cross biological barriers, like the blood-brain barrier, which prevents some medications from reaching the brain, is an advantage of employing these particles for medication administration. Additionally, research has demonstrated that nanobubbles enhance the delivery of medications to tumors, which can be challenging to target using conventional drug delivery systems.[18] Nanobubble delivery of pemigatinib is thus an unexplored field of research at the moment, but one that could be investigated in the future to enhance pemigatinib's PK and PD features. PLGA nanobubbles are poly(lactic-co-glycolic acid) nanobubbles. This biocompatible, biodegradable polymer is frequently utilized in medication delivery and biomedicine. PLGA nanobubble composition depends on the formulation. PLGA nanobubbles usually have a gas core and a polymer shell. The gas core can hold air, nitrogen, or carbon dioxide, depending on the purpose.PLGA and other materials can be added to nanobubble formulations to change their properties. Surfactants can stabilize nanobubbles and prevent coalescence. Nanobubble size, surface charge, and drug-loading capacity can be controlled with other additives. For biological applications like drug administration, imaging, and tissue engineering, PLGA nanobubble composition must be carefully tune.[19] Design of experiments (DoE) can optimize PLGA nanobubble composition for drug delivery. Researchers can discover how each component affects nanobubble size, surface charge, stability, and drug loading capability by systematically altering their composition. The goal is to find the best component combination for nanobubble characteristics and performance. A DoE research for PLGA nanobubbles can vary in polymer, surfactant, medication, pH, and preparation temperature. Depending on system complexity and the number of variables, the experiment can use a factorial or RSM design. DoE can identify the key nanobubble propertiesaffecting components and their relationships. The nanobubble composition can be optimized for drug loading, stability, and cancer treatment efficacy using this information.[20,21]

Materials And Methods

Materials

Aelida Pharmaceuticals, Haryana, India, supplied pemigatinib. The following materials were acquired from Sigma Aldrich Chemicals Private Limited, Bangalore, India: Cell culture medium, trypsin, newborn calf serum, poly(vinyl alcohol) (PVA), PLGA, and newborn calf serum. From Mumbai, India, S.D. Fine Chem. Pvt. Ltd. supplied the dichloromethane and perfluoropentane. The research relied solely on Millipore's Milli-Q water. The reagents and substances were of an analytical quality.

Methods

PLGA nanobubbles encapsulating pemigatinib

A customized water-in-oil-in-water (W/O/W) double emulsion, solvent diffusion-based evaporation method encapsulated pemigatinib in PLGA nanobubbles.[22] About 900 mg PLGA was made to dissolve in 10 mL dichloromethane and combined with 90 mg pemigatinib under sonication. Under optimal conditions in an ice bath,

a digital Sonifier® SFX150 (Branson Ultrasonic, Danbury, USA) emulsified this combination to generate the primary emulsion. The initial emulsion was immediately poured into a 20 mL 1% w/v PVA solution. Ultrasonic probe treatment at 30 W for 1-minute in darkness formed a double emulsion. After gently adding the emulsion to a 100 mL isopropanol solution (5% v/v), it was agitated at 2000 rpm for 5 hours at room temperature to separate dichloromethane. The blend was centrifuged for 10 minutes at 12,000 rpm. Centrifuged clear supernatant was removed, and precipitate was carefully splashed with de-ionized water, where centrifugation and washing was done thrice. Splashed nanobubbles were freeze-dried in the dark for 36 hours using LYPH LOCK 4.5 (Labconco Corporation, Kansas City). C_3F_8 gas was injected into the lyophilization chamber at 50 mL/min for 1-minute through a specific vial connector. Screw vials were sealed. Pemigatinib was successfully encapsulated within PLGA nanobubbles by this methodical process, making them available for future uses.

Ultrasound parameters optimization using RSM

- *DoEs*

Response surface methodology (RSM) is widely used to optimize ultrasonic operations since it fits mathematical models well. RSM, a statistical and mathematical method, is useful for creating prediction models that describe how various variables affect ultrasonic process outcomes. RSM captures and models complex system interactions and non-linearities, enabling accurate optimization for ultrasonic-based applications to improve efficiency and results.[23] The ultrasound operating parameters, determined during preliminary experiments, were 2.0 to 4.0 cm sonication distance, 3 to 5 minutes sonication time, 20 to 40% sonication amplitude, and 40 to 80 W sonication power. The vessels were sonicated for 5 seconds in an ice water bath. Sonicated samples were stored at 25°C in light-protected conditions. This study used CCD to assess the effects of sonication distance (A), amplitude (B), time (C), and power (D) regarding particle size and PDI. A factorial design at two levels (typically -1 and +1), center points for experimental errors, and axial points for response surface curvature are used. This design frequently varies factors (independent variables) at three levels: low (-1), center (0), and high (+1). The center points (0) are reproduced to measure experimental error and curvature. To estimate response surface curvature, axial points (coded -α and +α) are added. This architecture allows fitting a second-order polynomial equation to describe and optimize the response variable based on factors.[24] The general second-order polynomial equation for a four-factor CCD is:

$$Y = \beta_0 + \sum_{i=1}^{4} \beta_i X_i + \sum_{i=1}^{4} \beta_{ii} X_{ii}^2 + \sum_{i<j}^{4} \beta_{ij} X_i X_j + \varepsilon \quad (1)$$

Y -predicted response variable.
β_0 - model intercept.
β_i - linear coefficients showing the outcome of each factor.
β_{ii} - quadratic coefficients showing the effect of each factor squared.
β_{ij} - interaction coefficients representing the effect of interactions between various factors.
X_i and X_j are the levels of the independent variables (factors).
ε -error term.
Regression analysis estimates equation terms using CCD experimental data. The predictive polynomial equation models response variable behavior based on factors and their interactions using the coefficients ($\beta_0, \beta_i, \beta_{ii}$, and β_{ij}). The selected components and their quantities were determined by extensive preparatory tests (Table 1). The studies were conducted using a structured design, and Table 2 shows the dependent variable outcomes. Design-Expert software (Stat-Ease V13.0.5.0) was then utilized to examine the response surfaces within the investigational range.

- *Data analysis*

After the experiments, a complete statistical analysis was done to understand variable correlations. Several models described these relationships. To determine the best-fitting model, statistical measures such as model *p-value*, adjusted R^2, lack of fit *p-value*, regression coefficient (R^2), and coefficient of variation were carefully assessed. Model terms with a *p-value* greater than 0.005 are usually inconsequential and can be safely deleted, helping choose the most relevant and efficient model. We used backward elimination to remove independent variables that did not significantly affect our regression equation. This method included carefully eliminating non-contributing elements one by one. Three-dimensional RSM plots helped us grasp the link between selected response parameters and two independent variables. These plots graphically depicted functional relationships, revealing complex processes. We also used perturbation and contour plots to show

Table 1: Different levels of independent variables and goal of dependent variables

Independent factors	*Levels*				
	-α	*-1*	*0*	*+1*	*+α*
A – Sonication distance (cm)	1.59	2.0	3.0	4.0	4.41
B – Sonication time (min)	2.59	3	4	5	5.41
C – Sonication amplitude (%)	15.86	20	30	40	44.14
D – Sonication power (W)	31.72	40	60	80	88.28
Dependent variables	Goal				
Y1- Droplet size (nm)	Decrease				
Y2 – PDI	Decrease				

Table 2: Experiments as per the design and outcomes for the dependent variables

Expt	*A*	*B*	*C*	*D*	*Y1*	*Y2*
1	3	5.41	30	60	101.64	0.263
2	4	3	20	80	379.12	0.406
3	4	5	20	40	382.18	0.442
4	4	3	20	40	408.78	0.512
5	4	5	40	80	53.12	0.242
6	4.41	4	30	60	209.18	0.409
7	4	3	40	40	183.26	0.265
8	3	4	30	60	105.98	0.278
9	3	4	30	31.72	193.76	0.318
10	3	4	44.14	60	66.54	0.268
11	3	2.59	30	60	139.49	0.252
12	2	3	20	80	374.12	0.398
13	2	5	20	80	354.53	0.386
14	3	4	30	88.28	96.85	0.238
15	3	4	30	60	108.58	0.289
16	3	4	15.86	60	433.56	0.537
17	1.59	4	30	60	176.34	0.378
18	2	3	20	40	398.76	0.487
19	2	3	40	80	58.34	0.182
20	2	5	40	40	144.78	0.278
21	4	5	20	80	362.56	0.392
22	3	4	30	60	112.34	0.294
23	3	4	30	60	106.12	0.282
24	3	4	30	60	107.49	0.306
25	2	3	40	40	162.12	0.248
26	4	5	40	40	169.12	0.282
27	4	3	40	80	67.52	0.204
28	2	5	20	40	356.12	0.438
29	2	5	40	80	49.56	0.232
30	3	4	30	60	110.57	0.312

how independent variables affect response parameters. These graphs helped us understand the factors' effects, deepening our analysis.[25]

- *Optimization approach and verification*

We used numerical optimization to get the ideal independent variable values by constraining response parameters and influencing factors. These restrictions guided optimization to desired results.[26] After that, the prepared formulation was carefully manufactured in triplicate below ideal conditions. This method validated the optimization technique's efficacy and dependability, verifying that the optimal points produced the intended and consistent formulation results.

Characterization of prepared pemigatinib nanobubbles

- *Particle size, PDI, and ZP*

The particle size distribution of Pemigatinib nanobubbles was determined using the dynamic light scattering technique. The measurements were conducted at a constant angle of 90°. Prior to measurement, the samples were appropriately diluted with Milli Q water. The hydrodynamic diameter (Dh) and polydispersity index (PDI) of the particles were determined using cumulated analysis based on the average of three observations. The additional electrode was utilized to conduct ZP measurements on the same equipment, Mastersizer 2000, manufactured by Malvern Instruments Ltd, located in Worcestershire, UK. The trials were performed in triplicate at a temperature of 25 ± 2°C.

- *Drug payload and encapsulation effectiveness*

Percentage of pemigatinib encapsulated from the nanobubble preparation amount is called encapsulation efficiency. The drug's weight proportion in the nanobubble formulation is its payload.[27] In order to determine the concentration of pemigatinib in the formulation, a measured amount of the substance was dissolved in dichloromethane. The solution was then subjected to sonication for a duration of 10 minutes to facilitate the breakdown of any complex formations. Subsequently, the solution was diluted and analyzed using a UV spectrophotometer at a wavelength of 262 nm. "Drug payload" and "encapsulation efficiency" were estimated by means of equations 2 and 3:

$$\%\ Drug\ pay\ load = \frac{Weight\ of\ drug\ encapsulated\ in\ nanoformulation}{Weight\ of\ the\ NS\ formulation\ taken\ for\ analysis} \times 100 \quad (2)$$

$$\%\ Drug\ encapsulation\ efficiency = \frac{Weight\ of\ drug\ encapsulated\ in\ nanoformulation}{Initial\ weight\ of\ the\ drug\ fed\ for\ loading} \times 100 \quad (3)$$

- *Transmission electron microscopy*

Transmission electron microscopy (TEM) examined the morphology of both pemigatinib-loaded and plain nanobubbles. After applying a diluted nanoparticle suspension onto a film-coated copper grid, the grid was stained using a 2% (w/v) solution of phosphotungstic acid. The process of drying the sample increased the level of contrast. The study was conducted at a magnification of 25,000 times.

- *Fourier transformed infrared Spectroscopy and differential scanning calorimetry*

The spectra of pemigatinib, simple nanobubbles, and pemigatinib-loaded nanobubbles were obtained using a Tensor 27 FTIR Spectrophotometer by creating potassium bromide discs. Analyzed data was obtained within the spectral region of 4000 to 600 cm^{-1}. The Perkin Elmer DSC/7 differential scanning calorimeter, equipped with a

TAC 7/DX instrument controller, was employed to examine pemigatinib, plain nanobubbles, and nanobubbles filled with pemigatinib. The calibration of the melting point and heat of fusion was performed using indium. The samples in traditional aluminum pans were subjected to heating at a rate of 10°C per minute, starting at 30°C and reaching 400°C, while a nitrogen purge was maintained. The analysis of 5 mg samples was conducted on three separate occasions.

- *In-vitro drug release study and kinetics analysis*

Pemigatinib discharge from nanobubbles was measured *in-vitro* using dialysis bags at a temperature of 37°C. The release was observed for a duration of 24 hours utilizing a dialysis bag that had a molecular weight threshold of 12 to 14 kDa. Predefined time intervals were employed to substitute samples with a new phosphate buffer. We conducted three experiments. During the evaluation of a drug delivery system, research on drug release kinetics provides information on the mechanism and timing of drug release from a formulation, mathematical representations of drug release kinetics aid in elucidating and forecasting drug release.

- *Ultrasound stability of pemigatinib nanobubbles*

Ultrasound was used to stimulate pemigatinib-loaded nanobubbles at defined parameters and durations. Morphological analysis with optical microscopy assessed nanobubble structural integrity before and after ultrasonic exposure.

- *Stability studies of pemigatinib nanobubbles*

Pemigatinib nanobubble stability was tested for 1-month at 4, 25, and 40°C. Pemigatinib content, encapsulation efficiency, average particle size, and appearance were checked regularly to assess stability.

Determination of hemolytic activity

The hemolytic activity of PLGA nanobubbles was tested on human blood. Erythrocyte suspensions were treated at 37°C for 2 hours with various nanobubble percentages (v/v). The supernatant was analyzed at 543 nm after centrifugation.[28] Using an equation, the hemolysis percentage was computed versus 100% hemolysis control.

$$\%\ Hemolysis = \frac{ABS_{Sample} - ABS_0}{ABS_{100} - ABS_0}\ X\ 100 \qquad (4)$$

ABS_0 and ABS_{100} correspond to absorbances of at 0 and 100 %hemolysis of the solutions, correspondingly.

Cell culture

The American Type Culture Collection (ATCC, Manassas, VA, USA) gave MCF-7 cells, and Bogoo Biotech Co. Ltd. (Shanghai, China) graciously contributed Adriamycin-resistant MCF-7/ADR cells. To adapt to drug resistance, MCF-7/ADR cells were grown in a 500 ng/mL pemigatinib medium. In cultures, pemigatinib was increased to 1000 ng/mL. Later tests used these cells, which thrived and proliferated stably in a 1000 ng/mL pemigatinib culture media. All cells be developed at 37°C in a humidified 5% (CO_2) incubator in RPMI 1640 by 10% FBS, 100 U/mL penicillin, and 100 mg/mL streptomycin solution.

Cell viability-assay

A cell counting kit-8 (CCK-8) measured MCF-7 and MCF-7/ADR cell survival at the presence of free pemigatinib, plain nanobubbles, and pemigatinib nanobubbles. Using a 96-well plate, MCF-7/MCF-7/ADR cell suspensions got seeded at density 7 × 103 cells/well and adhered during the night at 37°C. Cells were cultured by free pemigatinib and nanobubbles (Pemigatinib concentrations: 5, 20, 40 µg/mL) for 72 hours after switching to fresh growth media. Each well was incubated for 1-hour with 10 mL of thawed CCK-8 solution. Absorbance was quantified at 450 nm by a microplate reader (Model 680, Bio-Rad, PA, USA). Comparing cell viability to nontreated cells was done as a percentage.

Cellular uptake of pemigatinib nanobubbles

MCF-7 cells were sown at 1.5×10^4 cells/well in 48 wells and allowed to attach for 24 hours.[29] Fresh culture medium with pemigatinib nanobubbles at 80, 160, and 240 µg/mL was added to wells and incubated for 6 hours. Other experimental groups examined time-dependent uptake. Pemigatinib nanobubbles (final concentration 40 µg/mL) were treated with cells for 4, 6, and 8 hours. All samples were cleaned three times with PBS and examined under a fluorescence microscope (TE-2000U, Nikon, Tokyo, Japan) after incubation.

Data presentation and statistical study

Data were presented as mean ± SEM, group differences were assessed using one-way ANOVA and Bonferroni testing, *p-value* < 0.05 indicates significance.

Results And Discussion

Nanobubbles, with their small size and core-shell composition, are promising medication delivery vehicles. They include gases or vaporizable chemicals like perfluorocarbons and are nanometer-sized. These structures have lipid, polymer, or albumin shells that stabilize the center. Nanobubbles are promising nanocarriers due to their stability, drug-loading capacity, and extravasation. Due to their small size, they may travel from blood arteries to tissues. Owing to their lesser size and unique physical features, polymer-shelled nanobubbles can enter the extravascular region, making them ideal for targeted medication administration. For nanobubble formulation, researchers have investigated biodegradable and non-biodegradable polymers. PLGA, a biocompatible and biodegradable polymer, is broadly used. PLGA is used for sutures, bone implants, screws,

and drug-release matrixes.[30] This work designed PLGA-shelled nanobubbles for pemigatinib delivery. We made nanobubbles from PLGA polymer with free carboxylic end groups. Perfluoropentane was used for the inner core and PLGA (50:50 ratios; intrinsic viscosity 0.22 dl/g, MW = 15000) for the shell to make blank and pemigatinib-loaded nanobubbles. However, the first trials showed variable particle size distribution, emphasizing the importance of parameters. Sonication distance (A) (the distance between the vessel bottom and the ultrasound probe) 2.0 to 4.0 cm, time (B) 3–5 minutes, amplitude (C) 20 to 40%, and power (D) 40 to 80 W significantly affected nanobubble particle size and PDI. Controlling nanobubble preparation variables made replicating these processes difficult. RSM is an efficient approach to optimizing solutions for desired outcomes.[31] Given its capacity to explore quadratic response surfaces and build accurate second-order polynomial models, CCD method was chosen to optimize preparation conditions.[32] The *p-values*, all under 0.05, displayed that the chosen model was very significant, notably for particle size and PDI. The λ_{max} of pemigatinib in acetonitrile was measured at 262 nm. The appearance, aroma, and taste of pemigatinib were described as white to off-white crystalline powder, pungent, and unpleasant. Pemigatinib melted at 95.5 to 98.5°C. The solubility of pemigatinib ranged from 30.66 µg/mL in water to 34132 µg/mL in dimethyl sulfoxide. Pemigatinib powder absorbed less than 0.5% moisture, proving its non-hygroscopicity.

RSM Optimization

Statistical analysis

A four-factor, five-level CCD was used for 30 studies. Table 2 shows the independent and dependent variables from these experiments. All trials had droplet sizes (Y1) of 49.56 to 433.56 nm and nanobubble PDI (Y2) of 0.182 to 0.537. The data was carefully analyzed using Stat-EaseDesignExpert® (V13.0.5.0) to determine the ANOVA, regression coefficients, and equations. A second-order quadratic model was fitted to the data to model the results. Table 3 shows best-fitting quadratic models with maximum F value. Table 4 summarises numerous linear regression analysis-derived mathematical equations for the variables. These polynomial equations show how each independent variable and their combined influence affect response variables. Individual independent variable coefficients demonstrate their effect on response variables. Multiple-variable and higher-order coefficients indicate interaction and quadratic effects correspondingly. Positive signs show synergy. However, negative signs designate antagonistic properties. The regression calculations all showed statistical significance.

In addition to coefficients, the lack of fit value is a crucial statistical measure for model fitness assessment. This is done by comparing residual error to duplicated center point pure error. A significantly low fit value indicates poor prediction efficiency. Therefore, a model having a non-significant lack of fit is crucial. Both quadratic models' non-significant lack of fit confirmed model fit. Every multiple linear regression analysis findings are summarised using R^2 value, adjusted R^2 value, and coefficient of variation. R^2 measures variation about the mean. R^2 values for both response variables were significantly larger than 0.985, indicating that the selected models explained experiment behavior. Additionally, the adjusted R^2 reading is critical to model sufficiency. High R^2 values do not necessarily designate model sufficiency because the number of variables can affect them. Adjusted R^2 value better indicates model-based competence. R^2 values for droplet size and PDI were 0.9978 and 0.9857, respectively. Both models' R^2 values and modified R^2 values were consistent, indicating that non-significant terms had been excluded. The coefficients of variation for both replies were 2.22 and 4.22, proving the results' repeatability and dependability. These values emphasize the study's legitimacy by demonstrating the experimental results' stability and consistency. Fig. 1 indicates that anticipated values and experimental results accord well. Each data point has a predicted value for all three replies. These images show that both models identified the procedure and formulation variables needed to make pemigatinib nanobubbles. The close agreement between projected and actual outcomes shows that the established models accurately and reliably capture the nanobubble preparation process's complexities.

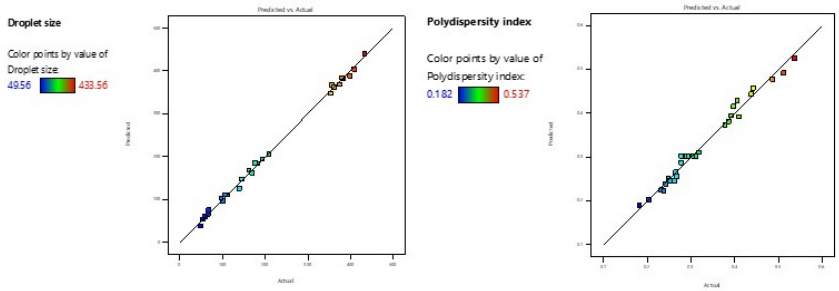

Fig. 1: Comparison among predicted and actual readings of size and PDI

Table 3: ANOVA of quadratic model for response droplet size (Y1) and PDI (Y2)

Source of variation	*Sum of squares*	*Degrees of freedom*	*Mean square value*	*F-value*	*p-value Prob>F*
Model	4.88×10^5	12	40651.74	2077.44	< 0.0001
A-Sonication distance	1182.3	1	1182.3	60.42	< 0.0001
B-Sonication time	2280.78	1	2280.78	116.56	< 0.0001
C-Sonication amplitude	3.50×10^5	1	3.50×10^5	17908.41	< 0.0001
D-Sonication power	20691.84	1	20691.84	1057.42	< 0.0001
CD	7886.77	1	7886.77	403.04	< 0.0001
A^2	16152.86	1	16152.86	825.47	< 0.0001
C^2	46055.67	1	46055.67	2353.6	< 0.0001
D^2	2981.73	1	2981.73	152.38	< 0.0001
Residual	332.66	17	19.57		
Lack of fit	300.59	12	25.05	3.91	0.0714
Pure error	32.07	5	6.41		
Cor total	4.88×10^5	29			
Model	0.2488	9	0.0276	116.62	< 0.0001
A-Sonication distance	0.001	1	0.001	4.13	0.0558
B-Sonication time	1.544×10^{-6}	1	1.544×10^{-6}	0.0065	0.9365
C-Sonication amplitude	0.1821	1	0.1821	768.3	< 0.0001
D-Sonication power	0.0194	1	0.0194	81.91	< 0.0001
BC	0.0049	1	0.0049	20.67	0.0002
A^2	0.0149	1	0.0149	62.89	< 0.0001
B^2	0.0073	1	0.0073	30.95	< 0.0001
C^2	0.0185	1	0.0185	77.85	< 0.0001
D^2	0.003	1	0.003	12.46	0.0021
Residual	0.0047	20	0.0002		
Lack of fit	0.0038	15	0.0003	1.44	0.3646
Pure error	0.0009	5	0.0002		
Cor total	0.2535	29			

Table 4: Regression equations for both results

Dependent variable	*Regression equation*
Y1	$110.77 + 7.69\ A - 10.68\ B - 132.37\ C - 32.17\ D - 22.20\ CD + 42.52\ A^2 + 71.16\ C^2 + 18.79\ D^2$
Y2	$0.3015 + 0.0070A + 0.0003\ B - 0.0954\ C - 0.0312\ D + 0.0175\ BC + 0.0400\ A^2 - 0.0280\ B^2 + 0.0445\ C^2 - 0.0178\ D^2$

Droplet size (Y1)

Since particle size affects nanobubble physical characteristics and stability, droplet size is an important quality control metric. Permeation and retention in tumor tissues and organs depend on nanocarrier size.[33] Table 2 shows nanobubble particle sizes of 49.56 to 433.56 nm. The polynomial model showed total factors (A, B, C, and D) affected nanobubble particle size. The droplet size quadratic model had an F-value of 1186.25, indicating its significance. Individual factors (A, B, C, and D), interacting term CD, and quadratic terms (A^2, C^2, and D^2) significantly affected droplet size (*p-value*s < 0.050). A "Lack of Fit F-value" of 10.19 indicated little significance. Non-significant misfit suggests a good model. The factorial equation for droplet size showed that C had a greater impact than D, B, and A, with R^2 and adjusted R^2 values of 0.9978 and 0.9970, correspondingly. The result shows that observed and expected values were similar. To determine the main and interacting impact of independent attributes on size, perturbation, 3D-surface, and contour graphs were created. The perturbation plot showed how A, B, C, and D affected droplet size. C affected droplet size the greatest, followed by D and B, with A having a slight influence (Fig. 2). Interactive and quadratic independent variable effects were shown via 3D RSM and contour graphs. Fig. 2 shows the interactive result of C and D (CD) at constant A and B on droplet size.

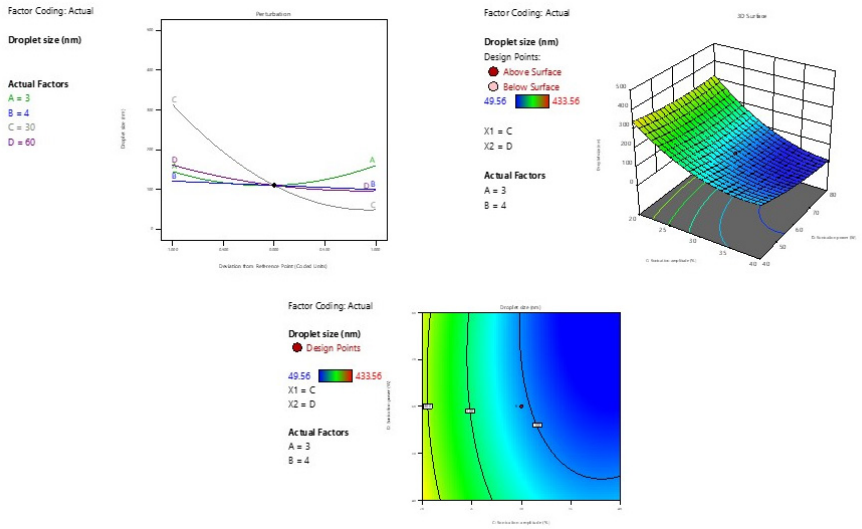

Fig. 2: Two-dimensional perturbation, 3D- RSM and Contour graph–Influence of A, B, C, and D-droplet size

PDI

The PDI characterizes a sample's particle size distribution. The width of the size distribution curve indicates particle size homogeneity or heterogeneity in a system. A lower PDI value indicates a more uniform size distribution in nanobubbles or nanoparticles. Conversely, a greater PDI value suggests a wider size distribution, meaning particles fluctuate more.[34] This investigation found nanobubble PDIs from 0.182 to 0.537, showing particle size variability. The polynomial model showed that variables C and D significantly affect nanobubble PDI. A high F-value of 116.62 indicated relevance in the PDI quadratic model. The factors C, D, BC, and quadratic terms A^2, B^2, C^2, and D^2 significantly affected PDI of nanobubbles ($p < 0.0500$). The model's "Lack of Fit F-value" of 1.44 indicated that lack of fit is not significant. A well-fitting model needs this non-significant fit difference. The factorial equation showed that variable C had a greater impact on PDI than D, A, and B, as indicated by a strong correlation coefficient (R^2) and adjusted R^2 values (0.9813 and 0.9729, correspondingly). The observed values' near match confirmed the model's accuracy. The perturbation plot showed that C had the greatest influence on PDI, followed by D with an intermediate effect and A and B with moderate effects (Fig. 3). The independent variables' interaction and quadratic impacts were shown via the 3D RSM and contour plots. Fig. 3 shows the interactive consequence of B and C (BC) at a steady A and D on PDI. Understanding and optimizing these variables, notably C and D, can help nanobubble compositions achieve a reduced PDI and a more homogenous particle size distribution, improving drug delivery efficiency and effectiveness.

Optimization process

We optimized process variables affecting response parameters using Derringer's desirability technique. Each response was converted to a desirability scale using Ymax and Ymin as goal functions (D). After a grid examination and viability analysis over the domain, desirability functions were combined into a geometric mean. Design-Expert software aided this method. A: 2.28 cm, B: 3.11 minutes, C: 40%, and D: 80 W yielded the highest attractiveness, resulting in a D rating of 1.000, indicating a great result (Table 5). Under these ideal conditions, three batches of nanobubbles were created to validate the model. Interestingly, the projected values and experimental results matched (Fig. 4). This proves that the CCD and Derringer's desirability approach optimize pemigatinib nanobubble formulation.

Characterization of nanobubble formulations

All batches of pemigatinib nanobubbles had consistent particle sizes and low PDI. High ZP showed nanobubble storage stability. The average particle size, PDI, and ZP of blank and pemigatinib-loaded nanobubbles. Strangely, blank and drug-loaded nanobubbles had similar particle sizes and PDI. PDI of blank nanobubbles and drug-loaded nanobubbles were found to be 0.168 ± 0.005 and 0.172 ± 0.005, respectively. TEM was used to analyze nanobubble morphology. TEM scans showed a 70 to 90 nm nanobubble surface shape and core-shell structure (Fig. 5). Comparing TEM and DLS particle sizes revealed an interesting finding. TEM, which visualizes at a microscopic level, measured particle sizes somewhat greater than DLS, which measures at a nanoscopic scale. High-resolution TEM imaging showed nanobubbles were 70 to 90 nm (Fig. 5). Encapsulation efficiency was 86.34% and loading capacity was 31.21% for pemigatinib in nanobubbles. Pemigatinib-loaded nanobubble aqueous suspension had a viscosity of 6.2 centipoise, which was appropriate for parenteral delivery. Significantly, pemigatinib loading into nanobubbles did not influence formulation viscosity.[27]

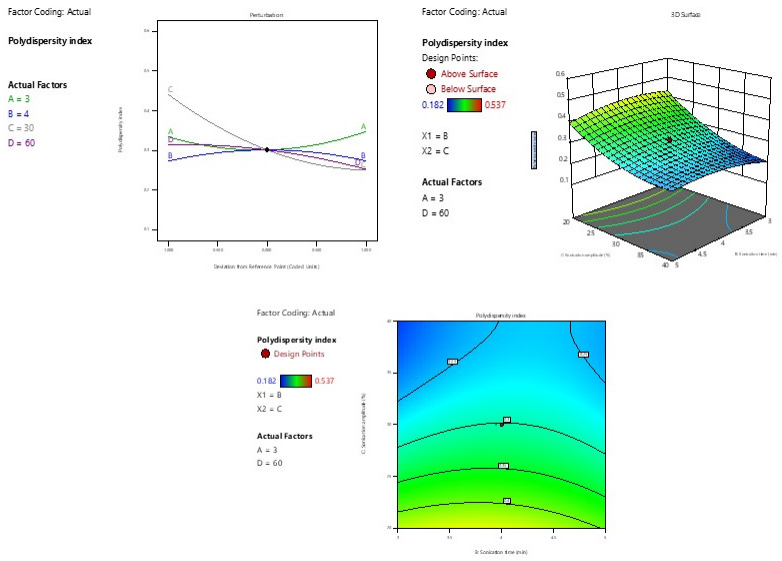

Fig. 3: 2-D perturbation, 3D- RSM and Contour graph– result of A, B, C and D on PDI

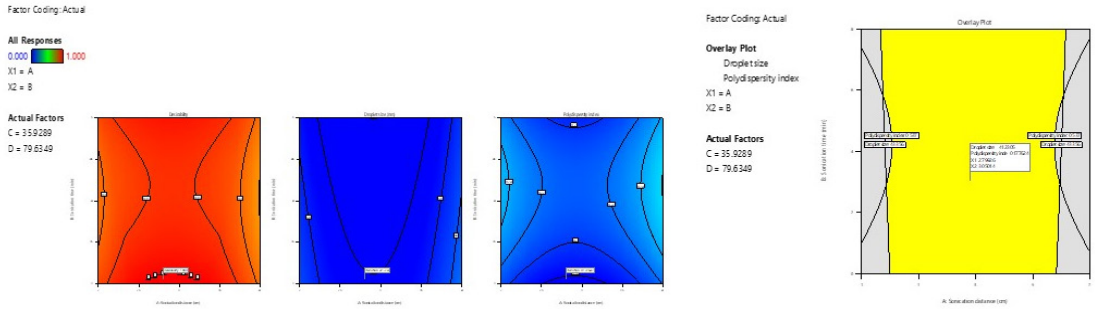

Fig. 4: Contour and overlay plots showing the global desirability value with point prediction

Table 5: Optimum circumstances achieved by affecting restrictions on response attributes

Independent attributes	*Optimized readings*	*Predicted readings*		*Actual values*		
		Y1 (nm)	*Y2*	*Batch*	*Y1 (nm)*	*Y2*
A: Sonication distance	2.28 cm	41.22	0.178	B1	42.36 ± 2.75	0.159 ± 0.0005
B: Sonication time	3.11 min			B2	38.53 ± 2.14	0.172 ± 0.0005
C: Sonication amplitude	40%			B3	37.18 ± 1.92	0.183 ± 0.0005
D: Sonication power	80 W					

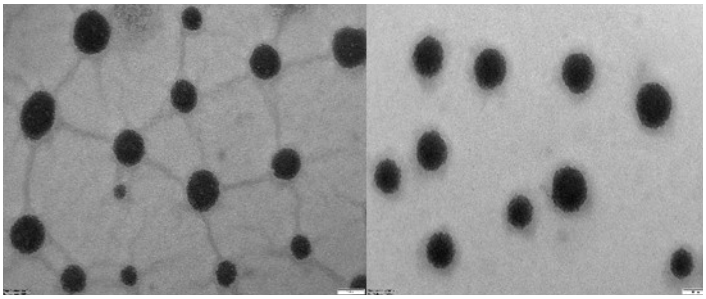

Fig. 5: TEM image of blank and pemigatinib-loaded nanobubbles

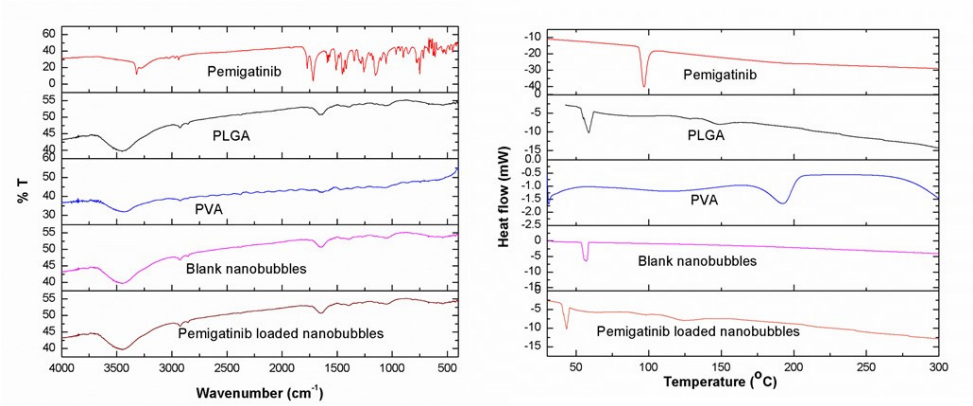

Fig. 6: FTIR and DSC spectra of pemigatinib, PLGA, blank nanobubbles, and pemigatinib loaded nanobubbles

Spectral analysis and thermal behavior

Fig. 6 compares the FTIR spectra of pemigatinib, PLGA, PVA, nanobubbles, and drug nanobubbles. FTIR spectra of pemigatinib-loaded nanobubbles did not show the drug's typical peaks, suggesting entrapment in the PLGA matrix. Fig. 6 shows the pemigatinib-loaded PLGA nanobubbles' DSC thermogram. Pure pemigatinib's DSC curve showed endothermic peak at 96.97°C, its melting temperature. Amorphous PLGA had no melting point on its thermogram. Polymer degradation was suggested by the large endothermic peak at 369.4°C. A significant endothermic peak at 212.6°C suggested PVA melting, while a minor hump at 40 to 42.5°C may represent the glass transition temperature. PLGA and PVA had similar melting transition values in blank and drug-loaded nanobubbles, suggesting the encapsulation technique did not change them. In the DSC examination, the absence of a crystalline drug material's sharp peak suggested the drug was imprisoned in the PLGA matrix. Drug formulation thermograms showed no endothermic peak, supporting this indication.

Fig. 7 displays the *in-vitro* pemigatinib release curve from nanobubbles in pH 7.4 phosphate buffer. Sonication, notably ultrasound, was tested for medication release from nanobubbles. Nanobubbles released more medication than the pemigatinib solution. Drug release with ultrasound help differed significantly from without. After 6 hours, sonication released 46.65% of pemigatinib, while 28.78% was released without. Ultrasound released 98.12% of pemigatinib over 24 hours, compared to 64.65% without. The data strongly suggested that ultrasound increases pemigatinib release from nanobubbles. The considerable increase in medication release under ultrasound suggests that nanobubble-based formulations can be modulated to optimize therapeutic effects. The mechanisms of this cavitation effect and its effects on drug delivery could be studied. To determine the drug release sequence and mechanism, optimized nanobubble formulation pemigatining release data was fitted into kinetic models. The Higuchi and Korsmeyer-Peppas models fit well,

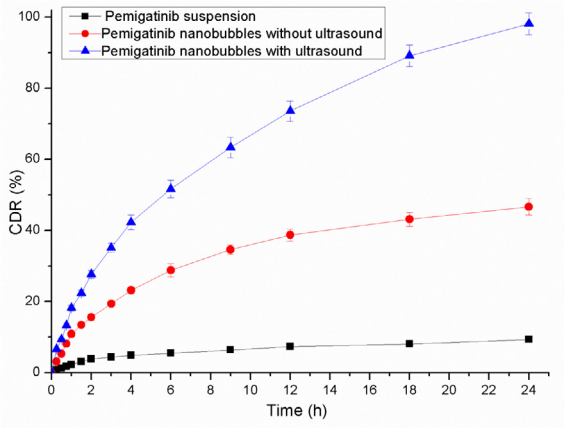

Fig. 7: *In-vitro* pemigatinib release outline with and without ultrasound support

indicating that drug discharge from the formulation is diffusion-controlled, which helps understand and optimize drug release from this formulation.

Ultrasound was used to test pemigatinib-loaded nanobubble stability at different temperatures. Nanobubbles' form and structure remained intact after 5 minutes of 2.5 MHz sonication at 25°C. At 37°C, nanobubbles began to shrink after 2 minutes of sonication and disappeared after 5 minutes, indicating destabilization. This indicates instability. Due to its low boiling point, perfluoropentane turns into a gas at 37°C. Nanobubbles' small size may change this transition temperature. Acoustic droplet creation occurs when ultrasound causes the gas central part to become a bubble from a nano-droplet. The storage stability of pemigatinib nanobubbles was tested at 4, 25, and 40°C for six months. Reports show pemigatinib content, encapsulation effectiveness, and size of pemigatinib nanobubbles at 0, 15, 30, 60, 120, and 180 days. Drug content did not change at 4 or 25°C. Encapsulation efficiency remained steady, especially at 4 and 25°C, stating that nanobubbles protected pemigatinib through degradation at usual storage temperatures. Encapsulation effectiveness decreased at 40°C, suggesting nanobubble

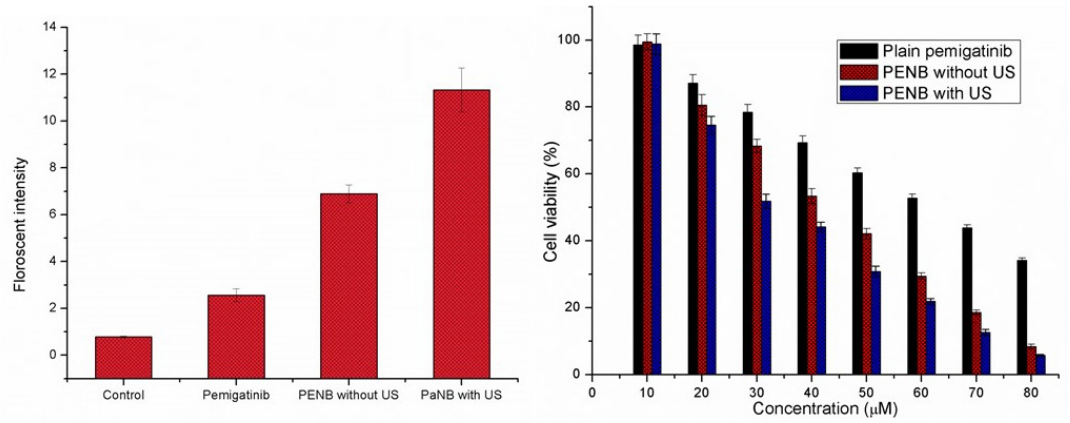

Fig. 8: Results of cellular uptake and *in-vitro* cytotoxicity of pemigatinib, pemigatinib nanobubbles devoid of ultrasound, and pemigatinib nanobubbles with ultrasound

structural instability due to rising temperature. The drug-loaded nanobubbles' PDI values remained below 0.2 during the stability testing. The formulation had a uniform and homogenous size distribution, confirming its stability and applicability. To assess safety of blank and pemigatinib nanobubbles, hemolytic action was measured. The hemolytic activity of PLGA nanobubble suspensions in water was examined. Even at 10 mg/mL, these nanobubbles were non-hemolytic. This shows that blank nanobubbles do not harm red blood cells, confirming their safety for use. Drug-loaded nanobubbles also displayed good safety for erythrocytes when tested for hemolysis. This reinforces the formulation's non-toxicity, confirming its parenteral safety.[28]

In-vitro cellular uptake study

MCF-7 cells, a common breast cancer cell line, were used to explore pemigatinib nanobubble absorption. Fluorescent intensity was measured for analysis. After a 2-hour incubation, MCF-7 cells were measured for fluorescence intensity. Cells treated with ultrasound and pemigatinib nanobubbles had a mean fluorescence intensity of 11.32 (Fig. 8). This intensity was around two times higher than in cells treated with pemigatinib nanobubbles alone, demonstrating that ultrasound greatly improved cellular absorption. This discovery shows that ultrasound can improve medication delivery, specifically pemigatinib cellular absorption, which could improve breast cancer therapy outcomes.

In-vitro cytotoxicity study

The MTT assay, a common cell survival and cytotoxicity test, was used to analyze pemigatinib-loaded nanobubbles' *in-vitro* cell toxicity against MCF-7 cells. The study examined the viability of MCF-7 cells bare to pemigatinib formulations at doses from 10 to 80 μM. At lower concentrations (10 μM), all pemigatinib formulations showed above 98% cell survival, indicating negligible cytotoxicity. At a concentration of 20 μM, cell viability still exceeded 75%. This may be because this concentration is below the minimal effective concentration for cytotoxicity. Ultrasound nanobubbles had the lowest cell viability as concentration rose. The quantity that inhibited 50% of cells was calculated as IC_{50}. Free pemigatinib showed an IC_{50} of 63.5 μM, while ultrasound-free and ultrasound-exposed nanobubbles had IC_{50} values of 42.38 and 30.87 μM, respectively (Fig. 8). This indicates that ultrasound-based nanobubbles unconfined pemigatinib into cells having high sensitivity and potential for cytotoxicity. The data suggest that this formulation may improve MCF-7 cell treatment outcomes, an important breast cancer treatment consideration.[29]

Conclusion

We created nanobubbles with a PLGA shell and perfluoropentane core to deliver pemigatinib, an anticancer medication. RSM helped us optimize formulation components for optimal particle size and homogeneous size distribution. Under precisely optimized settings, nanobubbles have remarkable particle size uniformity. Our investigation found that pemigatinib solubility affects medication efficacy. We found that pemigatinib in nanobubbles was more soluble than in suspension, especially at different pH levels. This increased solubility may improve therapeutic efficacy and BA. We performed *in-vitro* dissolution studies to confirm pemigatinib nanobubble benefits. The results were dramatic, showing superior dissolution profiles and gastrointestinal stability compared to standard suspension. This exciting result shows that nanobubble formulations of pemigatinib could significantly increase its oral BA, revolutionizing medication delivery for therapeutic impact. To assess pemigatinib nanobubble therapeutic potential, we conducted *in-vitro* cytotoxicity tests. Nanobubbles inhibited tumor cell development better, which was

encouraging. This shows that PLGA nanobubbles can be used in ultrasound-responsive formulations to deliver targeted drugs to fight cancer and other disorders. Our study shows that pemigatinib-loaded PLGA-shelled nanobubbles could revolutionize medication delivery. The improvements in solubility, dissolution characteristics, BA, and therapeutic efficacy show the potential of nanobubble-based drug delivery systems in oncology and beyond. More research in this area could lead to transformational medical therapeutic advances.

Acknowledgments

The authors show gratitude to the management of the department of Pharmacy, Bir Tikandrajit University, Canchipur, Imphal West, Manipur, India, for providing the research facilities. They are also grateful to the department head and principal of pharmaceutical sciences at TRR College of Pharmacy, Meerpet, Hyderabad, Telangana, India, for their encouragement and assistance.

References

1. Abou-Alfa GK, Sahai V, Hollebecque A, Vaccaro G, Melisi D, Al-Rajabi R, Paulson AS, Borad MJ, Gallinson D, Murphy AG, Oh DY, Dotan E, Catenacci DV, Cutsem EV, Ji T, Lihou CF, Zhen H, Feliz L, Vogel A. Pemigatinib for previously treated, locally advanced or metastatic cholangiocarcinoma: a multicentre, open-label, phase 2 study. Lancet Oncology. 2020;21(5):671-684. Available from: doi.org/10.1016/S1470-2045(20)30109-1.
2. Patel TH, Marcus L, Horiba MN, Donoghue M, Chatterjee S, Mishra- Kalyani PS, Schuck RN, Li Y, Zhang X, Fourie Zirkelbach J, Charlab R, Liu J, Yang Y, Lemery SJ, Pazdur R, Theoret MR, Fashoyin-Aje LA.FDA approval summary: Pemigatinib for previously treated, unresectable locally advanced, or metastatic cholangiocarcinoma with FGFR2 fusion or other rearrangement. Clinical Cancer Research. 202;29(5):838-842. Available from: doi.org/10.1158/1078-0432.CCR-22-2036.
3. Vogel A, Sahai V, Hollebecque A, Vaccaro G, Melisi D, Al-Rajabi R, Paulson AS, Borad MJ, Gallinson D, Murphy AG, Oh DY,Dotan E, Catenacci DV, Cutsem EV, Lihou CF, Zhen H, Feliz L, Abou- Alfa GK. FIGHT-202: A phase II study of pemigatinib in patients (pts) with previously treated locally advanced or metastatic cholangiocarcinoma (CCA). Annals of Oncology. 2019;30:v876. Available from: doi.org/10.1093/annonc/mdz394.031.
4. Rizzo A, Ricci AD, Brandi G. Pemigatinib: Hot topics behind the first approval of a targeted therapy in cholangiocarcinoma. Cancer Treatment and Research Communications.2021; 27:100337. Available from: doi.org/10.1016/j.ctarc.2021.100337
5. Reddy MR, Gubbiyappa KS. Formulation development, optimization, and characterization of Pemigatinib-loaded supersaturable self-nano emulsifying drug delivery systems. Future Journal of Pharmaceutical Sciences.2022;8(1):45. Available from: doi.org/10.1186/s43094-022-00434-4
6. Wu L, Zhang C, He C, Qian D, Lu L, Sun Y, Xu M, Zhuo J, Liu PC, Klabe R, Wynn R, Covington M, Gallagher K, Leffet L, Bowman K, Diamond S, Koblish H, Zhang Y, Soloviev M, Hollis G, Burn TC, Scherle P, Yeleswaram S, Huber R, Yao W. Discovery of pemigatinib: a potent and selective fibroblast growth factor receptor (FGFR) inhibitor. Journal of Medicinal Chemistry. 2021; 64(15):10666- 10679. Available from: doi.org/ 10.1021/acs.jmedchem.1c00713.
7. Al-Abboodi AS, Eid EE, Azam F, Al-Qubaisi MS. Inclusion complex of clausenidin with hydroxypropyl-fÀ-cyclodextrin: Improvedphysicochemical properties and anti-colon cancer activity. Saudi Pharmaceutical Journal. 2021;29(3):223-235. Available from: doi.org/10.1016/j.jsps.2021.01.006.
8. Bhalani DV, Nutan B, Kumar A, Singh Chandel AK. Bioavailability enhancement techniques for poorly aqueous soluble drugs and therapeutics. Biomedicines. 2022;10(9):2055. Available from: doi.org/ 10.3390/biomedicines10092055.
9. Satapathy S, Patro CS. Solid lipid nanoparticles for efficient oral delivery of tyrosine kinase inhibitors: a nano targeted cancer drug delivery. Advanced Pharmaceutical Bulletin. 2022; 12(2):298- 308. Available from: doi.org/ 10.34172/apb.2022.041.
10. Tian B, Hua S, Liu J. Cyclodextrin-based delivery systems for chemotherapeutic anticancer drugs: A review. Carbohydrate polymers. 2020; 232:115805. Available from: doi.org/ 10.1016/j.carbpol.2019.115805.
11. Fu Q, Lu HD, Xie YF, Liu JY, Han Y, Gong NB, Guo F. Salt formation of two BCS II drugs (indomethacin and naproxen) with (1R, 2R)-1, 2-diphenylethylenediamine: Crystal structures, solubility, and thermodynamics analysis. Journal of Molecular Structure. 2019;1185:281-289. Available from: doi.org/10.1016/j.molstruc.2019.02.104.
12. Sanches BM, Ferreira EI. Is prodrug design an approach to increase water solubility?. International Journal of Pharmaceutics. 2019;568:118498. Available from: doi.org/ 10.1016/j.ijpharm.2019.118498.
13. Winuprasith T, Koirala P, McClements DJ, Khomein P. Emulsion Technology in Nuclear Medicine: Targeted Radionuclide Therapies, Radiosensitizers, and Imaging Agents. International Journal of Nanomedicine. 2023;18:4449-4470. Available from: doi.org/10.2147/IJN.S416737
14. Abdifetah O, Na-Bangchang K. Pharmacokinetic studies of nanoparticles as a delivery system for conventional drugs and herb-derived compounds for cancer therapy: a systematic review. International Journal of Nanomedicine. 2019;14:5659-5677. Available from: doi.org/10.2147/IJN.S213229.
15. Jin J, Yang L, Chen F, Gu N. Drug delivery system based on nanobubbles. Interdisciplinary Materials. 2022;1(4):471-494. Available from: doi.org/10.1002/idm2.12050.
16. Pasupathy R, Pandian P, Selvamuthukumar S. Nanobubbles: A Novel Targeted Drug Delivery System. Brazilian Journal of Pharmaceutical Sciences.2022;58:e19608. Available from: doi.org/10.1590/s2175-97902022e19604
17. Kulkarni AD, Gulecha VS, Dolas RT, Zalte AG, Deore SR, Deore SS, Pande VV. Nanobubbles: Fundamentals and recent drug delivery applications. International Journal of Health Sciences. 2022;6(S8):1004.1025. Available from: doi.org/10.53730/ijhs.v6nS8.11598.
18. Jin J, Yang L, Chen F, Gu N. Drug delivery system based on nanobubbles. Interdisciplinary Materials. 2022;1(4):471-494. Available from: doi.org/10.1002/idm2.12050.
19. Gao J, Liu J, Meng Z, Li Y, Hong Y, Wang L, He L, Hu B, Zheng Y, Li T, Cui D. Ultrasound-assisted C3F8-filled PLGA nanobubbles for enhanced FGF21 delivery and improved prophylactic treatment of diabetic cardiomyopathy. Acta Biomaterialia. 2021;130:395-408. Available from: doi.org/10.1016/j.actbio.2021.06.015.
20. Rampado R, Peer D. Design of experiments in the optimization of nanoparticle-based drug delivery systems. Journal of Controlled Release. 2023;358:398-419. Available from: doi.org/10.1016/j.jconrel.2023.05.001.
21. Struzek AM, Scherlies R. Quality by Design as a Tool in the Optimisation of Nanoparticle Preparation-A Case Study of PLGA Nanoparticles. Pharmaceutics. 2023;15(2):617-622. Available from: doi.org/10.3390/pharmaceutics1502061.
22. Iqbal M, Zafar N, Fessi H, Elaissari A. Double emulsion solvent evaporation techniques used for drug encapsulation. International Journal of Pharmaceutics. 2015;496(2):173-190. Available from: doi.org/10.1016/j.ijpharm.2015.10.057.
23. Candioti LV, De Zan MM, Camara MS, Goicoechea HC. Experimental design and multiple response optimization. Using the desirability function in analytical methods development. Talanta. 2014;124:123-138. Available from: doi.org/10.1016/j. talanta.2014.01.034.

24. Njoku CN, Otisi SK. Application of Central Composite Design with Design Expert v13 in Process Optimization. Intech Open. 2023. Available from: doi.org/ 10.5772/intechopen.109704.
25. Bhattacharya S. Central Composite Design for Response Surface Methodology and Its Application in Pharmacy. Response Surface Methodology in Engineering Science. Intech Open. 2021 Jan 28.
26. Paterakis NG, Gibescu M, Bakirtzis AG, Catalao JP. A Multi-Objective Optimization Approach to Risk-Constrained Energy and Reserve Procurement Using Demand Response. IEEE Transactions on Power Systems. 2018;33(4):3940-3954. Available from: doi.org/10.1109/TPWRS.2017.2785266.
27. Zhang X, Zheng Y, Wang Z, Huang S, Chen Y, Jiang W, Zhang H, Ding M, Li Q, Xiao X, Luo X. Methotrexate-loaded PLGA nanobubbles for ultrasound imaging and synergistic targeted therapy of residual tumor during HIFU ablation. Biomaterials. 2014;35(19):5148-5161. Available from: doi.org/10.1016/j.biomaterials.2014.02.036
28. Yedgar S, Barshtein G, Gural A. Hemolytic Activity of Nanoparticles as a Marker of Their Hemocompatibility. Micromachines (Basel). 2022;13(12):2091. Available from: doi.org/10.3390/mi13122091.
29. Wang S, Liu X, Chen S, Liu Z, Zhang X, Liang XJ, Li L. Regulation of Ca2+ signaling for drug-resistant breast cancer therapy with mesoporous silica nanocapsule encapsulated doxorubicin/siRNA cocktail. ACS Nano. 2018;13(1):274-283. Available from: doi.org/10.1021/acsnano.8b05639.
30. Xu JS, Huang J, Qin R, et al. Synthesizing and binding dual-mode poly (lactic-co-glycolic acid) (PLGA) nanobubbles for cancer targeting and imaging. Biomaterials. 2010;31(7):1716-1722. Available from: doi.org/10.1016/j.biomaterials.2009.11.052.
31. Brzezi.ska R, Wirkowska-Wojdy.a M, Piasecka I, Gorska A. Application of Response Surface Methodology to Optimize the Extraction Process of Bioactive Compounds Obtained from Coffee Silverskin. Applied Sciences.2023;13(9):5388. Available from: doi.org/10.3390/app13095388.
32. Ahmed Z, Mehmood T, Ferheen I, Noori AW, Almansouri M, Waseem M. Optimization of exopolysaccharide produced by L. kefiranofaciens ZW3 using response surface Methodology. International Journal of Food Properties. 2023;26(1):2285-2293. Available from: doi.org/10.1080/10942912.2023.2245577
33. Danaei M, Dehghankhold M, Ataei S, Hasanzadeh Davarani F, Javanmard R, Dokhani A, Khorasani S, Mozafari MR. Impact of particle size and polydispersity index on the clinical applications of lipidic nanocarrier systems. Pharmaceutics. 2018;10(2):57. Available from: doi.org/10.3390/pharmaceutics10020057.
34. Teixeira MI, Lopes CM, Goncalves H, Catita J, Silva AM, Rodrigues F, Amaral MH, Costa PC. Formulation, characterization, and cytotoxicity evaluation of lactoferrin functionalized lipid nanoparticles for riluzole delivery to the brain. Pharmaceutics. 2022;14(1):185. Available from: doi.org/10.3390/pharmaceutics14010185.

HOW TO CITE THIS ARTICLE: Nandini P, Bhikshapathi DVRN, Viswaja M, Mamatha P. Development and Characterization of Ultrasound-assisted PLGA Nanobubbles for the Triggered Delivery of Pemigatinib by Design of Experiments. Int. J. Pharm. Sci. Drug Res. 2024;16(3):399-411. **DOI:** 10.25004/IJPSDR.2024.160312